Comparative Study on The Properties of CuInSe₂ and CuGaSe₂ Thin Films

İdris Candan[1, 3*], Hasan Hüseyin Güllü[2, 3]

[1] Department of Physics, Kocaeli University, 41380, Izmit, Kocaeli, Turkey (ORCID: 0000-0002-9950-713X)
[2] Department of Electrical and Electronics Engineering, Atılım University, 06836, Ankara, Turkey (ORCID: 0000-0001-8541-5309)
[3] The Center for Solar Energy Research and Applications (GUNAM), METU, 06800, Ankara, Turkey

Abstract

Two edge of $Cu(In_{1-x}Ga_x)Se_2$ (CIGS) thin film semiconductors for x=0 ($CuInSe_2$) and x=1 ($CuGaSe_2$) have been produced onto the soda lime glass substrates at 250 °C by sputtering from Cu, InSe and GaSe targets. The effects of In and Ga ratio and the post-annealing at 350 °C and 400 °C on the properties of $CuInSe_2$ (CIS) and $CuGaSe_2$ (CGS) thin film samples have been investigated. The structural properties of the deposited films have been examined by using X-ray diffraction (XRD) and the compositions of samples were analyzed by performing energy dispersive X-ray diffraction analysis (EDXA) techniques. Raman spectra of thin film samples were studied at room temperature to determine the Raman active modes. The most intensive line (A_1 modes) at 178 cm⁻¹ and 185 cm⁻¹ were observed for CIS and CGS thin films annealed at 400 °C, respectively. This is the most active mode detected in the Raman spectra of this type of chalcopyrite structures. For as-grown and annealed CGS thin films at 350 °C , the line 486 cm⁻¹ was observed however intensity of this line decreased with increasing annealing temperature and totally disappeared after annealing at 400 °C. Optic transmission measurements showed that the deposited CIS and CGS thin films have optic band gap values for as grown and annealed (at 400 °C) samples changing from 1.28 eV to 1.45 eV and from 1.68 eV to 1.75 eV respectively. The room temperature electrical conductivities of the samples were measured as 8.6×10^{-3} and 13.6×10^{-2} $(\Omega.cm)^{-1}$ for n-type CIS thin film samples; 1.6 and 1.9 $(\Omega.cm)^{-1}$ for p-type CGS thin film samples before and after annealing at 400 °C, respectively.

Keywords: CIS, CGS, Thin films, Sputtering, XRD, Raman Spectroscopy.

CuInSe₂ ve CuGaSe₂ İnce Filmlerin Özellikleri Üzerine Karşılaştırmalı Çalışma

Öz

$Cu(In_{1-x}Ga_x)Se_2$ (CIGS) yarıiletken ince filmlerin iki kenar noktası olan x=0 ($CuInSe_2$) ve x=1 ($CuGaSe_2$) ince filmleri, Cu, InSe ve GaSe hedeflerden saçtırma yöntemi ile 250 °C sıcaklıkta soda lime cam alttaşlar üzerine kaplandı. In ve Ga oranı ve üretim sonrası ısıl işlemin $CuInSe_2$ (CIS) ve $CuGaSe_2$ (CGS) ince filmlerin özellikleri üzerine etkileri araştırıldı. Üretilmiş filmlerin yapısal özelliklerini

* Corresponding Author: Department of Physics, Kocaeli University, 41380, Izmit, Kocaeli, Turkey, ORCID: 0000-0002-9950-713X, idriscandan@gmail.com

incelemek için X-ışını kırınımı (XRD) ve örneklerin bileşenleri enerji dağılımlı X-ışını kırınımı analizi (EDXA) yöntemi kullanılarak analiz edildi. İnce film örneklerinin Raman aktif modlarının tayini için oda sıcaklığında Raman spektroskopi ölçümleri yapıldı. 400 ºC sıcaklıkta ısıl işlem uygulanmış CIS ve CGS ince film örneklerinin en aktif modları (A_1 modu) en yoğun çizgilerin sırayla 178 cm^{-1} ve 185 cm^{-1} olduğu gözlendi. Bu mod kalkopirit yapıların Raman spektroskopisinde gözlemlenen en güçlü moddur. Isıl işlem uygulanmamış ve 350 ºC'ta ısıl işlem uygulanmış CGS örneklerinde 486 cm^{-1} çizgisi gözlenmiş olmasına rağmen bu çizginin yoğunluğu artan ısıl işlem sıcaklığı ile ters orantılı olarak azaldığı ve 400 ºC uygulanan ısıl işlem sonrası tamamen yok olduğu gözlenmiştir. Üretilen CIS ve CGS ince filmlerin optik geçirgenlik ölçümleri sonucunda ısıl işlem uygulanmayan filmler ve at 400 ºC sıcaklıkta ısıl işlem uygulanan filmler için optik bant aralıklarındaki değişim değerleri CIS için 1.28 eV ile 1.45 eV, CGS için 1.68 eV ile 1.75 eV aralıklarında değiştiği hesaplandı. Numunelerin oda sıcaklığındaki elektriksel iletkenlikleri ısıl işlem öncesi ve 400 ºC ısıl işlem sonrasında n-CIS için sırayla 8.6x10^{-3} ve 13.6x10^{-2} (Ω.cm)$^{-1}$, p-CGS için sırayla 1.6 and 1.9 (Ω.cm)$^{-1}$ olarak ölçüldü.

Anahtar Kelimeler: CIS, CGS, İnce Filmler, Saçtırma, XRD, Raman Spektroskopisi.

1. Introduction

Polycrystalline chalcopyrite CuIn$_{1-x}$Ga$_x$Se$_2$ (CIGS) thin film is one of the appropriate materials for high-efficiency photovoltaic (PV) devices because of desirable band gap for solar cell applications. The recorded laboratory efficiency of CIGS polycrystalline thin film based solar cells has exceeded 22.9 % (K.K. 2015). The structural, optic and electrical properties of CIGS thin film changes with various parameters such as the proportions of Cu/(In+Ga) and Ga/(In+Ga) or In/(In+Ga) and/or film thickness (Zhang et al. 1998; Caballero & Guillen 2003). It was detected that with increasing contribution of Ga, the conduction band minimum increases as a result of enlargement of the band gap of CIGS thin film, while the valence band maximum of it decreases marginally (Chaure et al. 2005). It is possible to adjust the band gap values by scanning CuIn$_{1-x}$Ga$_x$Se$_2$ compound as a function of x in the range of 0-1 (Fan et al. 1982). The quaternary CIGS compound materials have been grown on various substrates by different methods such as electron beam evaporation (e-beam evaporation) (Venkatachalam et al. 2008; Ramanathan et al. 2005; Li et al. 2011), reactive magnetron sputtering (Gillespie et al. 1997), thermal evaporation (Klenk et al. 2002; F. Smaïli et al. 2008), thermal co-evaporation (Niemi et al. 1996; Basol et al. 2000; Kushiya et al. 1995), flash evaporation (Ahmed et al. 1998), pulsed laser deposition (PLD) (Levoska et al. 1994; Matsubara et al. 2003) and physical vapor transport (Bhattacharya et al. 1999). Furthermore, thin layers of CIGS are regarded as the most encouraging material for high-efficiency and low-priced solar cells, due to their stability against photo-erosion and high absorptivity (>10^{5}cm^{-1}) (Chaure et al. 2005). Additionally, The CuInSe$_2$ (CIS) and CuGaSe$_2$ (CGS) compounds are of special interest because of their suitability for near infra-red region (NIR), solar cell applications, non-linear optics in IR, sensors, detectors (Shay & Wernick 1975; Chichibu et al. 2004; Botha et al. 2003).

The focus of this research is to examine the changes in the structural, optic and electrical properties of chalcopyrite CuIn$_{1-x}$Ga$_x$Se$_2$ (CIGS) thin film samples for x=0 (CIS) and x=1 (CGS), produced by the sputtering method and the effects of the post-heat treatment procedure at different temperatures on the film properties.

2. Experimental Details

CIS and CGS chalcopyrite thin films have been produced onto the chemically cleaned soda-lime glass substrates by the sequential sputtering growth method using the Cu, InSe and GaSe targets. During production, the substrate temperature was kept at 250 oC and Inficon XTM/2 thickness controller was used to follow the thickness of the deposited films. Following to the depositions, Dektak 6M profilometer was used to check the thickness of the samples electromechanically and the values were measured around 500 nm (±10 nm) for CIS and CGS samples. In order to find out the effects of post annealing process on the deposited samples, the thin films were annealed at the temperature of 350 oC and 400 oC for 30 minutes under the atmosphere of nitrogen. Rigaku Miniflex XRD system equipped with radiation source of CuKα was used to measure X-ray diffraction (XRD) profiles of produced CIS and CGS samples. The compounds of the deposited film samples were measured by using JSM-6400 Scanning Electron Microscope (SEM) equipped with NORAN 6 X-ray Microanalysis System. The measurements of confocal Raman spectra were performed by Jobin Yvon Horiba confocal Raman and excitation source provided by 532 nm Nd:YAG laser at room temperature. Peltier cooled CCD detector and double monochromator were used to designate Raman shifts. Optic characterizations of the thin films were performed by transmittance measurements using a Shimadzu UV-1201 spectrophotometer in the wavelength region 350-1100 nm. For the electrical measurements, high-purity indium (In) was evaporated to apply the ohmic contacts on the thin films by evaporation technique through the copper masks in cloverleaf geometry. The temperature dependent dark- and photo-conductivity measurements of the deposited thin films were done in a Janis liquid nitrogen cryostat under vacuum and the temperature of samples was followed and controlled by using Lake-Shore 331 temperature controller in between 100 - 400 K.

3. Results and Discussion

3.1. Compositional Analysis

The elemental compositions of deposited CIS and CGS thin films were determined by EDXA measurements taken from different part of the sample surfaces and average values were listed in Table 1. As observed from Table 1, annealing processes resulted in the systematic decrease in Se, increase in Cu, and In (or Ga) compositions for CIS and CGS thin film samples. This can be accepted as the indication of re-evaporation or segregation of Se with the post annealing process (De Blasi et al. 1989).

Table 1. *EDXA results of as-grown and annealed CIS and CGS samples.*

Sample	Cu (%)	In (%)	Ga (%)	Se (%)
CIS As-grown	20.7	31.4	-	47.9
CIS A 400 ºC	23.5	36.8	-	39.7
CGS As-grown	24.7	-	30.6	44.7
CGS A 400 ºC	26.7	-	35.6	37.7

3.2. Structural Analysis

Figure 1 (a) and **Figure 1 (b)** show the XRD patterns of CIS and CGS thin film samples, respectively. Both as-grown CIS and CGS thin film samples were observed to have amorphous structure. However, after annealing at 400 ºC for CIS and at 350 ºC for CGS under nitrogen atmosphere, they showed polycrystalline behavior as observed in **Figure 1 (a)** and **(b)**. XRD diffractograms indicate that the most intense peaks of the deposited CIS and CGS films were around 26.6º and 27.4º respectively and the preferred orientation direction was along (112) plane (Klenk et al. 2002; Chichibu et al. 1998; Steichen et al. 2011). The crystallinity of the thin film samples increased with increasing annealing temperature as seen from the **Figure 1 (a)** and **(b)**. Structural analyses with XRD showed that CIS and CGS films had the tetragonal zinc-blende structure with the lattice constants of a, b : 5.8 Å, c: 11.6 Å and a, b : 5.6 Å, c: 11.2 Å, respectively (Jaffe & Zunger 1983; Fearheiley et al. 1985; Abrahams & Bernstein 1974).
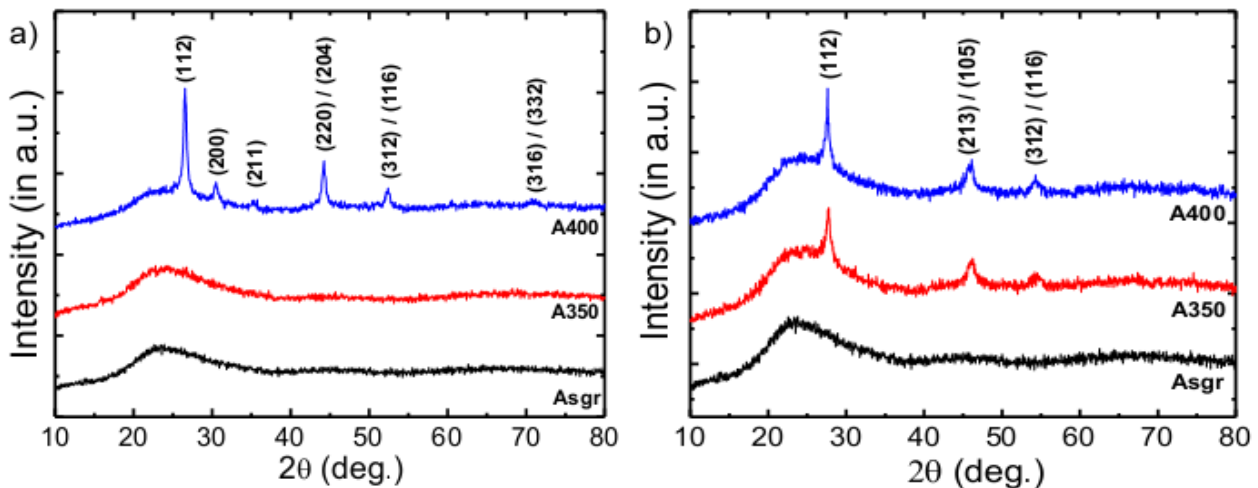
Figure 1. *X-ray diffraction patterns of as-grown and annealed **(a)** CIS and **(b)** CGS thin films at 350 and 400 ºC.*

Although the as-grown CIS and CGS samples were observed to have amorphous structure, the switch to the polycrystalline phase from the amorphous took place with annealing. The reason for the switch the amorphous structure to polycrystalline phase might be the production of samples at low temperature, since the impinged atoms prefer to place at constant location because of the nucleation processes during the production and deficient thermal energy for the movement, and the transition to the polycrystalline phase might be triggered by thermal heating process (De Blasi et al. 1989).

On the other hand, the observed peaks at 2θ~44.1° and 45.6° were identified as the main peaks of $Cu_{2-x}Se$ phase along (220)/(204) and (213)/(105) directions. The enhancement of crystallinity was observed with increasing annealing temperature because of the decreasing in structural disarrangement with ascending annealing temperature. In addition, the weakly bounded selenium atoms in the structure were possibly freed and separated to the surface of samples with increasing annealing temperatures (see **Table 1**) (Julien et al. 1990; Thomas & Kutty 1990). The Scherrer's formula was used to calculate the by using the value of main XRD peak's full width half maximum (FWHM) (Langford & Wilson 1978). The values of grain size were detected to be in between 160 and 205 nm for CGS thin films increasing with ascending annealing temperature. The enlargement in the grain size is the confirmation of the advance of the crystallinity with the annealing procedure as detected in X-ray diffraction pattern of CGS thin films. However, the grain size of the CIS thin film annealed at 400 °C was calculated as 206 nm since below this annealing temperature it showed amorphous behavior as observed from XRD patterns.

3.3. Raman Analysis

The crystal structure of chalcopyrite CIGS is related to the space group, I$\bar{4}$2d, i.e. to the point group D_{2d}^{12} (Choi 2011; Roy et al. 2002). In the naturel vibration for group D_{2d}, the primitive cell's oscillations containing acoustic modes and optic modes are split as follows;

$$\Gamma_\alpha = A_1 + 2A_2 + 3B_1 + 4B_2 + 7E \tag{1}$$

The number of Raman active modes $A_1 + 2A_2 + 3B_1 + 3B_2 + 6E$ is 19 and the symmetry of acoustic modes is B_2+E (Rincón & Ramírez 1992). The tetragonal ternary (I-III-VI$_2$) composition can be imagined as two permeate face centered cubic (fcc) lattice, the initial anion lattice takes place group VI atoms and the other being an ordered draw up group I and group III cations. Accordingly, super lattice structure cuts down the cubic zinc blende (sphalerite) symmetry to that of a tetragonal chalcopyrite structure (A_I B_{III} C_{IV}) (Albin et al. 1988). Two structural differences are in existence between the chalcopyrite and sphalerite structures. These differences are;

- The tetragonal deformation (c/a ratio) is not equivalent to 2.0.
- The group VI atoms displacement of from their ideal value of u=25, here u being the tetrahedral deformation (Roy et al. 2002).

In this work, Raman spectra of samples were performed at room temperature to find out the active modes of Raman in CIS and CGS the thin film samples.
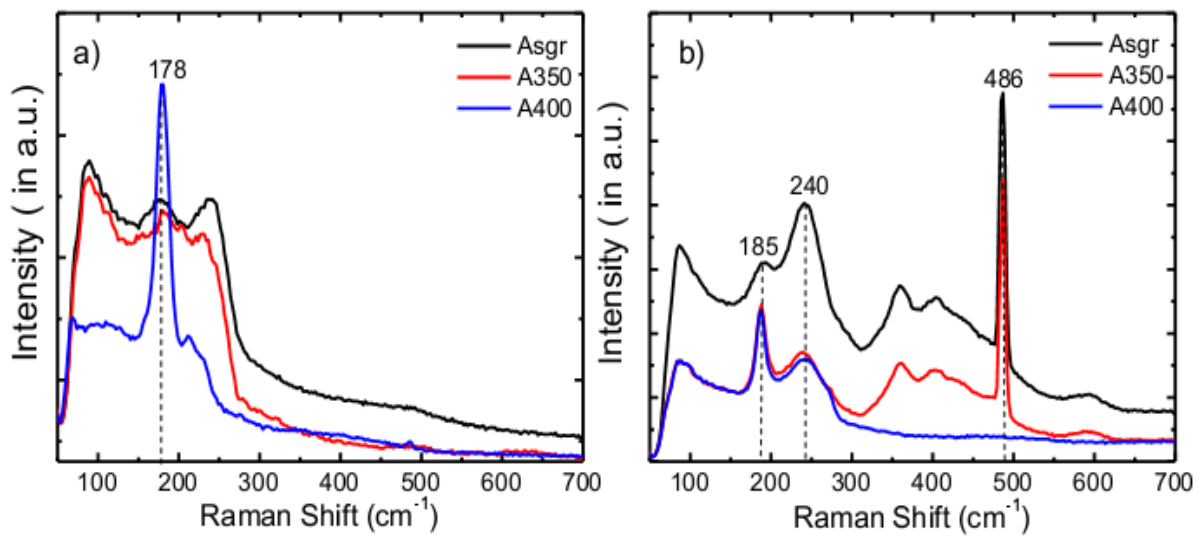
Figure 2. Raman spectra of as-grown and annealed (a) CIS and (b) CGS samples at 350 and 400 °C.

Figure 2 (a) and **Figure 2 (b)** show the Raman spectra of CIS and CGS thin films recorded at room temperature, respectively. For 400 °C annealed CIS thin films, the most concentrated line at 178 cm^{-1} might be allocated to the A1 mode, that is the most powerful

mode, detected in the Raman spectra of chalcopyrite structure (Tanino et al. 1992). Moreover, as-grown and annealed CGS thin film sample at 350 ºC has the most intensive line at 486 cm^{-1}. **Figure 2 (b)** exhibits that the intensity of peak at 486 cm^{-1} decreases with annealing and disappears. After annealing at 400 ºC, CGS sample has a strong peak at 185 cm-1. This peak is the powerful line of A1 mode that might be the result of the separation of Se atom in the structure (De Blasi et al. 1989). The existence of the phase of Cu$_{2-x}$ Se at 240 cm^{-1} was observed in as-deposited and annealed CGS films at 350 ºC. However, this phase totally disappeared after annealing at 400 ºC. Apparently, the heat treatment has the significant effect on the crystallinity and the component of the deposited films. The results of Raman spectra were coherent with the results of XRD as shown in the previous part.

3.4. Optical Analysis

In order to find out the optic properties of the thin film samples, transmittance measurements were performed at room temperature in the wavelength value of 350-1100 nm and absorption coefficient was computed by using the equation;

$$\alpha = \frac{1}{d} Ln\left(\frac{I_0}{I}\right) \qquad (2)$$

here d being the film thickness, I being the transmitted light intensity, and I$_0$ being the incident light vertical to the sample surface. After computing the absorption coefficient in the analyzed spectral domain, Tauc plot (Touc 1974) was used to compute the optic band gap, E$_g$, values in accordance with the following relation;

$$(\alpha h v) = A\left(h v - E_g\right)^n \qquad (3)$$

here A being a constant and n being the power exponent that varies with regard to the types of transition, as for direct transition n = 1/2 , and for indirect transition *n =2* (Pankove 1971). One may decide the type of direct or indirect transition by plotting $(\alpha h v)^{1/n}$ versus hv. In order to obtain the E$_g$ values of CIS and CGS thin film samples, $(\alpha h v)^2$ versus hv were plotted due to CIS and CGS thin films have direct optic transition (Jaffe & Zunger 1983). **Figure 3 (a)** and **Figure 3 (b)** illustrate the typical plot of transmission versus wavelength for CIS and CGS thin film samples, respectively.
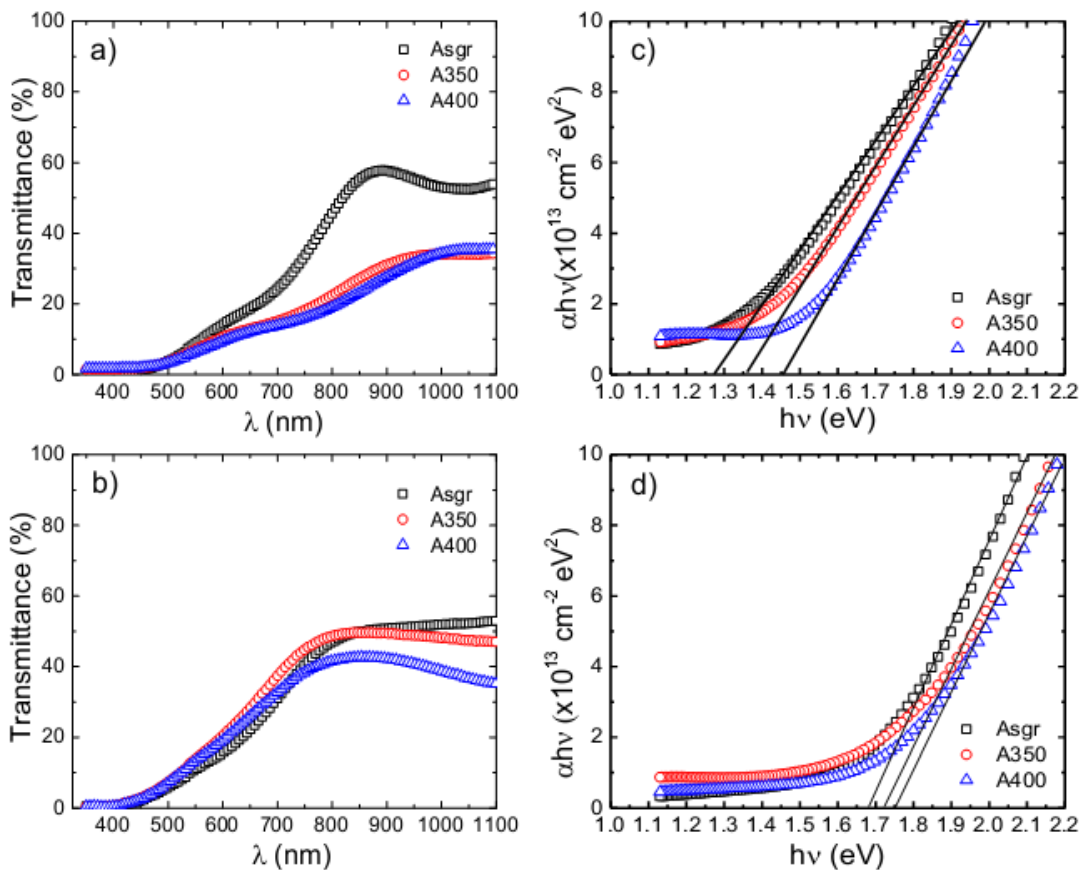
Figure 3. *Transmission spectra for as-grown and annealed (a) CIS and (b) CGS thin films at 350 and 400 ºC. The variation of (αhv)²*
as a function of incident photon energy for as-grown and annealed (c) CIS and (d) CGS thin films at 350 and 400 ºC.

As shown in **Figure 3 (a)**, there is significant change in transmission with the annealing temperature. Transmittance value significantly increases following the annealing at 400 °C for CIS thin film sample. On the other hand, there is not significant change in transmission values of CGS thin film sample. **Figure 3 (c)** and **Figure 3 (d)** show the plot of $(\alpha h\nu)^2$ versus $(h\nu)$ for the as-grown and annealed CIS and CGS thin film samples at 350 and 400 °C, respectively. The band gap values were calculated from the linear regression of the least squares fit to the plot of $(\alpha h\nu)^2$ versus $(h\nu)$ on the energy axis $(h\nu)$ and were tabulated in **Table 2** for the as-grown and annealed CIS and CGS thin films.

Table 2. *The calculated band gap values for the as-grown and annealed CIS and CGS thin films at 350 and 400 °C.*

Sample	E_g (eV)		
	As-grown	**A 350 °C**	**A 400 °C**
CIS	1.28	1.36	1.45
CGS	1.68	1.72	1.75

As seen from **Table 2**, the band gap values are lying in between 1.28 eV and 1.45 eV for as grown and annealed CIS thin films and between 1.68 eV and 1.75 eV for as-deposited and annealed CGS thin films. There is a considerable enlargement in the band gap values of CIS samples during the conversion from amorphous phase to polycrystalline phase occurs with annealing between 350 and 400 °C. The optic band gap value of CIS firstly increases from 1.28 to 1.34 eV with annealing at 350 °C, and then demonstrates a similar step up to 1.45 eV with annealing at 400 °C. The same kind of increasing behavior was also observed in CGS samples. Such as, initially, the band gap energy was 1.68 eV for as-grown sample, and then it increased slightly from 1.72 to 1.75 eV with increasing annealing temperature from 350 °C to 400 °C. In the amorphous form of CIS samples, the density of defects and the degree of disorder are more prominent than in polycrystalline phase (Mott & Davis 1971). Generally, the defect density and the decrease in disorder in the structure lead to a raise in the optic band gap energy. Additionally, other possible reason for observing enhance in band gap with increasing annealing temperature might be the impregnation of suspended bonds in the amorphous structure (Mott & Davis 1971). Therefore, the behavior of shifting of band gap to the higher energy edge found while the phase alteration from amorphous to crystalline phase may also be associated with CIS and CGS thin films crystallization. C. Julien et al. (Julien et al. 1990) and B. Thomas et al. (Thomas & Kutty 1990) informed a similar event for InSe thin films. The increase in optic band gap value with increasing annealing temperature was assigned to the loss of Se at high temperatures along with the creation of different phases (De Blasi et al. 1989; Thomas & Kutty 1990; Julien et al. 1990). The optic absorption coefficient was computed from the transmission data (**Figure 3 (a)** and **(b)**) and the room temperature absorption coefficient values for all samples were found to be about 10^5 - 10^6 cm^{-1} for the incident light in the range of 350-1100 nm (Kazmerski et al. 1983).

3.5. Electrical Analysis

The hot probe measurements indicated that CIS films have n-type and CGS thin films have p-type electrical conductivity (Chichibu et al. 2004; Neumann et al. 1978). The temperature dependent conductivity measurements for as-deposited and annealed CIS and CGS samples at 400 °C were performed in between 100-400 K. In order to eliminate the finite contact effects, a Cu-mask in the geometry of van der Pauw was used to deposit the thin film samples. I-V measurements were measured for the films to check the ohmicity of In contacts before the electrical measurements.
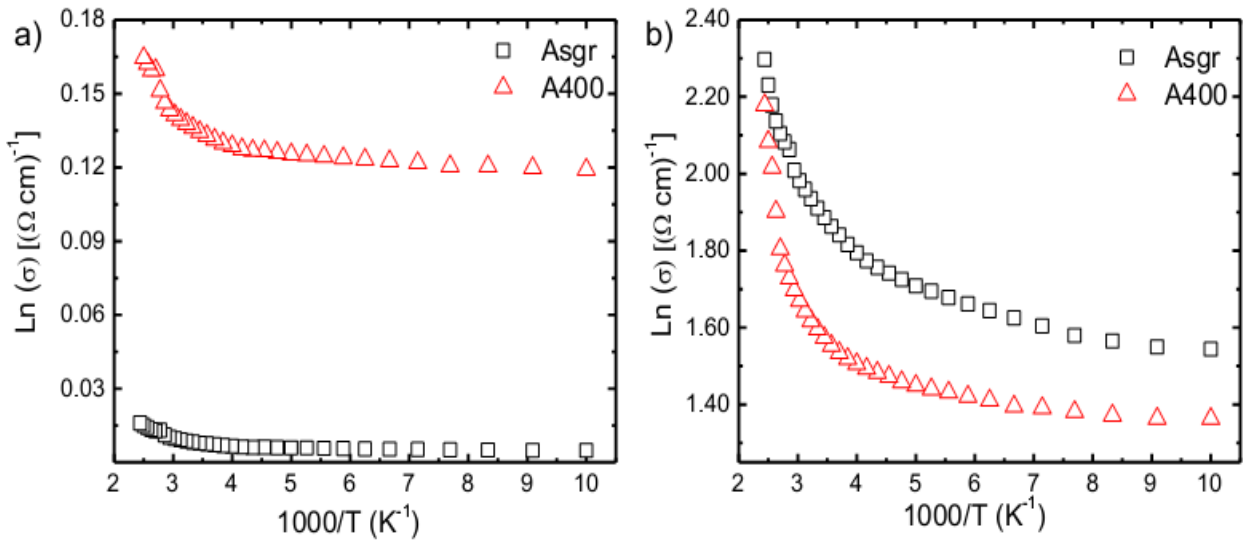
Figure 4. *Deviation of conductivity with reverse temperature for as-grown and annealed (a) CIS and (b) CGS thin films at 400 ^{o}C.*

As shown in **Figure 4 (a)** and **Figure 4 (b)**, the room temperature electrical conductivity values of both CIS and CGS films increase systematically with increasing annealing temperature. The room temperature conductivity values were 8.6×10^{-3} and 13.6×10^{-2} $(\Omega.cm)^{-1}$ for CIS films; 1.6 and 1.9 $(\Omega.cm)^{-1}$ for CGS films before and after post-annealing process, respectively. The variation of conductivity with the absolute temperature in between 100-400 K, for both CIS and CGS thin film samples does not show any sharp behavior. The reason for this type of electrical conductivity-temperature variation could be related to the metal rich composition of the films consistent with the results obtained from the compositional analysis which showed that the samples had Se-deficient and Cu_2In (or Ga)-rich compositions.

4. Conclusions

Thin films of $CuIn_{1-x}Ga_xSe_2$ (CIGS) with x=0 (CIS) and x=1 (CGS), were deposited by sputtering onto glass substrates and the structural, optic, electrical properties of the deposited films were investigated as a function of the post annealing temperatures. The compositional analyses showed that Se content of the samples decreases with increasing annealing temperature and Se-deficient and Cu, In (or Ga)-rich thin film structures were detected. XRD measurements indicated that as-grown CIS and CGS thin films had an amorphous structure and the conversion from the amorphous to the polycrystalline phase was seen following the annealing at 350 ^{o}C and 400 ^{o}C with the preferred crystalline orientation in the direction of (112) plane for both structures. The grain sizes of all samples were increased with annealing. The room temperature Raman measurements of the samples indicated that the main Raman peaks were at 178 cm^{-1} and 185 cm^{-1} for CIS and CGS, respectively. In as-grown and annealed CGS films at 350 ^{o}C, the peak at 240 cm^{-1} because of the vibration mode of $Cu_{2-x}Se$ phase was observed and disappeared after annealing at 400 ^{o}C. The band gap values were found as 1.28 eV for as-grown and 1.45 eV for annealed CIS; and 1.68 eV for as-grown and 1.75 eV for annealed CGS thin film samples. The optic and electrical properties of the samples showed different behavior depending on the advancement in the crystallinity and modification of the films structure. Electrical measurements indicated that the room temperature electrical conductivity values of both n-CIS and p-CGS films increase systematically with increasing annealing temperatures.

Acknowledgements

References

Abrahams, S.C. & Bernstein, J.L., 1974. Piezoelectric nonlinear optic $CuGaSe_2$ and $CdGeAs_2$: Crystal structure, chalcopyrite microhardness, and sublattice distortion. The Journal of Chemical Physics, 61(3), pp.1140–1146.

Ahmed, E. et al., 1998. Significance of substrate temperature on the properties of flash evaporated $CuIn_{0.75}Ga_{0.25}Se_2$ thin films. Thin Solid Films, 335(1–2), pp.54–58.

Albin, D. et al., 1988. Composition-structure relationships for multisource evaporated $CuGaSe_2$ thin films. Journal of Applied Physics, 64(10), pp.4903–4908.

Basol, B.M. et al., 2000. Studies on sulfur diffusion into Cu(In,Ga)Se_2 thin films. Progress in Photovoltaics, 8(2), pp.227–235.

Bhattacharya, R.N. et al., 1999. Thin-film $CuIn_{1-x}Ga_xSe_2$ photovoltaic cells from solution-based precursor layers. Applied Physics Letters, 75(10), pp.1431–1433.

De Blasi, C. et al., 1989. Optical absorption and structure of thermally annealed gallium selenide thin films. Journal of Applied Physics, 65(3), pp.1164–1167.

Botha, J.R., Branch, M.S. & Weber, J., 2003. Steady state and time-resolved photoluminescence characterisation of copper gallium disulphide. Thin Solid Films, 431–432(03), pp.210–213.

Caballero, R. & Guillen, C., 2003. Optical and electrical properties of $CuIn_{1-x}Ga_xSe_2$ thin films obtained by selenization of sequentially evaporated metallic layers. Thin Solid Films, 431(03), pp.200–204.

Chaure, N.B. et al., 2005. Electrodeposition of p+, p, i, n and n+-type copper indium gallium diselenide for development of multilayer thin film solar cells. Thin Solid Films, 472(1–2), pp.212–216.

Chichibu, S. et al., 1998. Band gap energies of bulk, thin-film, and epitaxial layers of $CuInSe_2$ and $CuGaSe_2$ band gap energies of bulk, thin-film, and epitaxial layers of. Journal of Applied Physics, 83(7), p.3678.

Chichibu, S.F. et al., 2004. Greenish-white electroluminescence from p-type $CuGaS_2$ heterojunction diodes using n-type ZnO as an electron injector. Applied Physics Letters, 85(19), p.4403.

Choi, I.H., 2011. Raman spectroscopy of $CuIn_{1-x}Ga_xSe_2$ for in-situ monitoring of the composition ratio. Thin Solid Films, 519, pp.4390–4393.

F. Smaïli, Kanzari, M. & Rezig, B., 2008. Characterization of $CuIn_{1-x}Al_xS_2$ thin films prepared by thermal evaporation. Materials Science and Engineering C, 28(5–6), pp.954–958.

Fan, J.C.C., Tsaur, B.Y. & Palm, B.J., 1982. Optimal design of high-efficiency tandem cells. In 16th Photovoltaic Specialists Conference, San Diego, CA (IEEE, New York). pp. 692–701.

Fearheiley, M.L. et al., 1985. The lattice constants of $CuInSe_2$. Journal of Electronic Materials, 14(6), pp.677–678.

Gillespie, T.J., Miles, A. & del Cueto, J.A., 1997. Reactive magnetron sputtering of transparent and conductive zinc oxide films deposited at high rates onto CIS/CIGS photovoltaic devices. In 26th PVSC, Anaheim, CA. pp. 3–6.

Jaffe, J. & Zunger, A., 1983. Electronic structure of the ternary chalcopyrite semiconductors $CuAlS_2$, $CuGaS_2$, $CuInS_2$, $CuAlSe_2$, $CuGaSe_2$, and $CuInSe_2$. Physical Review B, 28(10), pp.5822–5847.

Julien, C., Benramdane, N. & Guesdon, J.P., 1990. Transformation steps of structure in flash-deposited films of a-InSe. Semiconductor Science and Technology, 5, pp.905–910.

Kazmerski, L.L. et al., 1983. Optical properties and grain boundary effects in $CuInSe_2$ Optical properties and grain boundary effects in $CuInSe_2$. Journal of Vacuum Science & Technology A, 1(2), p.395.

Klenk, M. et al., 2002. Preparation of device quality chalcopyrite thin films by thermal evaporation of compound materials. Semiconductor Science and Technology, 17(5), pp.435–439.

Kushiya, K. et al., 1995. Development of High-Efficiency $CuIn_xGa_{1-x}Se_2$ Thin-Film Solar Cells by Selenization with Elemental Se Vapor in Vacuum. ". Jpn. J. Appl. Phys. Vol. 34, pp. 54-60, 1995, 34, pp.54–60.

Langford, J.I. & Wilson, A.J.C., 1978. Scherrer after sixty years: A survey and some new results in the determination of crystallite size. Journal of Applied Crystallography, 11(2), pp.102–113.

Levoska, J. et al., 1994. Pulsed laser ablation deposition of CuInSe2 and $CuIn_{1-x}Ga_xSe_2$ thin films. Physica Scripta, T54, pp.244–247.

Li, Z.H., Cho, E.S. & Kwon, S.J., 2011. Properties of the Cu(In,Ga)Se_2 absorbers deposited by electron-beam evaporation method for solar cells. Current Applied Physics, 11(1), pp.28–33.

Matsubara, K. et al., 2003. ZnO transparent conducting films deposited by pulsed laser deposition for solar cell applications. Thin Solid Films, 431–432(03), pp.369–372.

Mott, N.F. & Davis, E.A., 1971. Electronic Processes in Non-Crystalline Materials, Oxford University Press, London.

Neumann, H. et al., 1978. Electrical properties of n-type $CuInSe_2$ single crystals. Solid State Communications, 25, pp.899–902.

Niemi, E. et al., 1996. Small- and large-area CIGS modules by co-evaporation. In Conference Record of the Twenty Fifth IEEE Photovoltaic Specialists Conference - 1996. IEEE, pp. 801–804.

Pankove, J.I., 1971. Optical Processes in Semiconductors, Dover Publications Inc., New York.

Ramanathan, K. et al., 2005. Properties of high-efficiency $CuInGaSe_2$ thin film solar cells. Thin Solid Films, 480–481, pp.499–502.

Rincón, C. & Ramírez, F.J., 1992. Lattice vibrations of $CuInSe_2$ and $CuGaSe_2$ by Raman microspectrometry. Journal of Applied Physics, 72(9), pp.4321–4324.

Roy, S. et al., 2002. Characterization of Cu (In, Ga)Se_2 films by Raman scattering. Materials Chemistry and Physics, 73, pp.24–30.

Satoshi Yoshida, 2017. Solar Frontier Achieves World Record Thin-Film Solar Cell Efficiency of 22.9%. *Online*, pp.2–3. Available at: http://www.solar-frontier.com/eng/news/2015/C051171.html.

Shay, J.L. & Wernick, J.H., 1975. Ternary chalcopyrite semiconductors, Pergamon, Oxford.

Steichen, M., Thomassey, M. & Dale, P.J., 2011. Controlled electrodeposition of Cu – Ga from a deep eutectic solvent for low cost fabrication of $CuGaSe_2$ thin film solar cells. Phys. Chem. Chem. Phys, 13, pp.4292–4302.

Tanino, H. et al., 1992. Raman spectra of $CuInSe_2$. Physical Review B, 45(23), pp.13323–13330.

Thomas, B. & Kutty, T.R.N., 1990. Formation of Single-Phase Indium Selenide Thin Films by Elemental Evaporation. Physica Status Solidi (a), 119(1), pp.127–138.

Touc, J., 1974. Amorphous and Liquid Semiconductors, Springer, New York.

Venkatachalam, M. et al., 2008. Effect of annealing on the structural properties of electron beam deposited CIGS thin films. Thin Solid Films, 516(20), pp.6848–6852.

Zhang, S.B. et al., 1998. Defect physics of the $CuInSe_2$ chalcopyrite semiconductor. Physical Review B, 57(16), pp.9642–9656.

0000-0001-8541-5309